DOI: 10.21062/mft.2025.083 http://www.journalmt.com

Characterization of Microstructure and Defects in the Ti-6Al-4V Alloy Produced by 3D Printing SLM Technology

Kateřina Caldová (0009-0003-8106-2878)[1], Andrea Školáková (0000-0002-7436-9252)[1,2], Jan Pinc (0000-0001-9581-3204)[1,2], Dalibor Vojtěch (0000-0002-6910-3206)[1]

[1]Department of Metals and Corrosion Engineering, University of Chemistry and Technology, Prague, Technická 5, 166 28 Prague 6, Czech Republic. E-mail: sindelan@scht.cz, vojtechd@vscht.cz

[2]FZU – The Institute of Physics of the Czech Academy of Sciences, Na Slovance 1999/2, Prague 8, 182 21, Czech Republic. E-mail: skolakova@fzu.cz, pinc@fzu.cz

The Ti-6Al-4V alloy is widely used as a material for medical implants. In the future, it may be employed for 3D printing using the selective laser melting method. The advantages of 3D printing are for example production of complex shapes or ability to create customized implants. One of the disadvantages of this method is the deterioration of mechanical properties, particularly the ductility of the alloy, caused by high residual stress resulting from rapid cooling during printing. This article aims to characterize the microstructure and defects of the printed alloy and the impact of hot isostatic pressing. Optical microscopy, scanning electron microscopy, and micro-computed tomography were utilized for the study. It was found that the heat treatment has a significant effect on the pore size and microstructural transformation. These findings could lead to the optimization of the manufacturing process and improve the quality of implants made from this alloy.

Keywords: Selective laser melting (SLM), Ti-6Al-4V alloy, Defects, Pores, Hot isostatic pressing (HIP)

1 Introduction

The Ti-6Al-4V alloy is one of the most widely used titanium alloys, representing approximately 50% of total titanium production [1]. Its primary applications are in the aerospace industry and in medicine [2,3]. This alloy is distinguished by its low density while maintaining high strength, as well as excellent corrosion resistance and bio-compatibility [4, 5].

Thanks to these properties, the alloy has found broad application across various medical fields. In dentistry, it is used for dental bridges and other types of fixation implants. In orthopedics, it serves as the structural material for joint replacement implants and for bone stabilization or replacement. It is also widely used in other medical fields, such as screws, meshes, stents, spinal fixation devices, and heart pumps [6].

Processing of the alloy is energy-intensive and costly. For this reason, numerous additive manufacturing (AM) methods have been developed [7]. One promising technique for producing titanium implants is Selective Laser Melting (SLM) [8], a type of powder bed fusion process. SLM involves repeated layering and selective melting of thin powder layers into the desired geometry using a laser beam [7-11]. The unsintered powder assists in dissipating excess heat [12] and simultaneously provides structural support, thereby reducing the need for additional sup-port structures [8, 10].

During 3D printing, specific types of defects may form. Since SLM-produced components are often intended for direct use in load-bearing applications, minimizing the number of defects and pores is critical. Stress concentrations within these defects directly affect mechanical properties [13]. The most common defect types associated with SLM include gas pores, lack-of-fusion defects, and keyholes [14, 15].

Each defect type is characterized by a typical size and shape. Gas pores are usually spherical, with diameters exceeding 50 μm, and typically exhibit an aspect ratio greater than 0.7 [15]. Lack-of-fusion defects are larger and have irregular shapes, often around 100 μm in size. They may also contain unsintered powder particles [15].

The most effective method for reducing SLM-related defects is Hot Isostatic Pressing (HIP). By applying high pressure and elevated temperature, HIP promotes pore closure and microstructural changes [16], resulting in improved mechanical performance.

Samples fabricated using SLM, as well as those subsequently processed by HIP, were examined. The effect of HIP was investigated with respect to the quantity and size of defects, the transformation of microstructure, and their influence on the mechanical properties. Due to the inferior mechanical properties of as-printed samples, which limit their suitability for implantology, HIP appears to be a promising post-processing method to improve these properties and thus enable their potential use in biomedical applications.

2 Experimental

The samples were prepared by Selective Laser Melting (SLM). The starting material was Ti-6Al-4V powder from Dentaurum (DE) with particle sizes ranging from 15 to 45 μm and an average particle size of 30 μm. The samples were fabricated by the company Prospon spol. s.r.o. using the M2 Cusin Concept-Laser printer. The laser power was set to 200 W, scanning speed to 800 $mm \cdot s^{-1}$, hatching distance to 112 μm, layer thickness to 30 μm, and printing was performed under a protective argon atmosphere.

For analysis, two sets of five samples were printed in the shape of rods with smooth cylindrical heads. The to-tal length of each sample was 50 mm, with a gauge length 20 mm long and a diameter of 3 mm. The samples were printed in an upright position. Batch number 2 was processed by hot isostatic pressing (HIP) at 900 °C and 150 MPa for 2 h in a protective argon atmosphere.

Prior to the analysis, the samples were subjected to tensile testing. For further examination, the grip sections were removed and used for subsequent analyses. Firstly, volumetric analysis of internal defects was performed using Zeiss micro-computed tomography (μCT), followed by data processing with Dragonfly software and OpePNM plugin [17].

Subsequently, the samples were embedded in epoxy resin and ground using a Struers LaboPol-25 grinder with silicon carbide (SiC) abrasive papers ranging from P60 to P4000 grit. They were then polished using a Struers LaboPol-5 polisher and neoprene cloth with a SiO_2 suspension (Eposil F with H_2O_2 (30 %) in a 1:6 volume ratio).

After polishing, the samples were rinsed with distilled water and ethanol, and then dried. The microstructure was observed using a Zeiss Axio Observer D1m optical microscope. The surface of the unetched samples was observed at 50x magnification for surface area porosity and quantification of defects, which was subsequently evaluated using ImageJ software.

For microstructure visualization, samples were etched in Kroll's reagent (5 mL HNO_3, 10 mL HF, and 85 mL H_2O) for a few seconds, then rinsed with distilled water and ethanol, and dried. The microstructure was observed using a light microscope at magnifications ranging from 50x to 1000x.

Finally, the samples were cleaned in acetone using ultrasound for 1 min, mounted on aluminum stubs using silver paste, and observed with an FEI QUANTA 3D scanning electron microscope (SEM) equipped with an energy-dispersive X-ray spectrometer (EDS) and electron backscatter diffraction (EBSD) detector.

3 Results and discussion

3.1 Mechanical properties

First, the mechanical properties of both batches were measured. The results are presented in Tab. 1. Based on the mechanical testing results, these series were selected for subsequent analysis and comparison with the standards relevant to the use of the Ti-6Al-4V alloy in implantology.

The first batch was printed using the SLM method and analysed in the as-built state. Batch number 2 was also printed by SLM and subsequently processed by HIP. According to ASTM F1472, the samples are required to exhibit a minimum yield strength of 860 MPa, ultimate tensile strength of 930 MPa, and ductility of 10 %.

All samples met the requirements for yield strength and ultimate tensile strength. However, samples 1–5 from batch number 1 and sample 8 from batch number 2 exhibited insufficient ductility.

Tab. 1 *Mechanical properties of samples*

Batch number	Sample number	Elastic modulus [GPa]	Yield strength [MPa]	Ultimate tensile strength [MPa]	Ductility [%]
1	1	108	1028	1051	5
	2	107	1027	1051	3
	3	109	1029	1050	4
	4	107	1026	1047	5
	5	108	1027	1049	4
2	6	107	960	1029	15
	7	108	961	1037	17
	8	106	970	1026	4
	9	110	963	1033	16
	10	106	969	1038	16

3.2 Microstructure

The microstructure and defects were characterized by optical and scanning electron microscopy. The longitudinal sections of the samples after etching were analysed.

Defects were observed under an optical microscope (Figs. 1 a – c). A significant number of defects were de-tected in the first batch. The samples contained different types of defects, including gas pores (Fig. 1b) and lack of fusion (Fig. 1c). Only micropores

were observed in the second batch (Fig. 2b), which was treated by HIP.

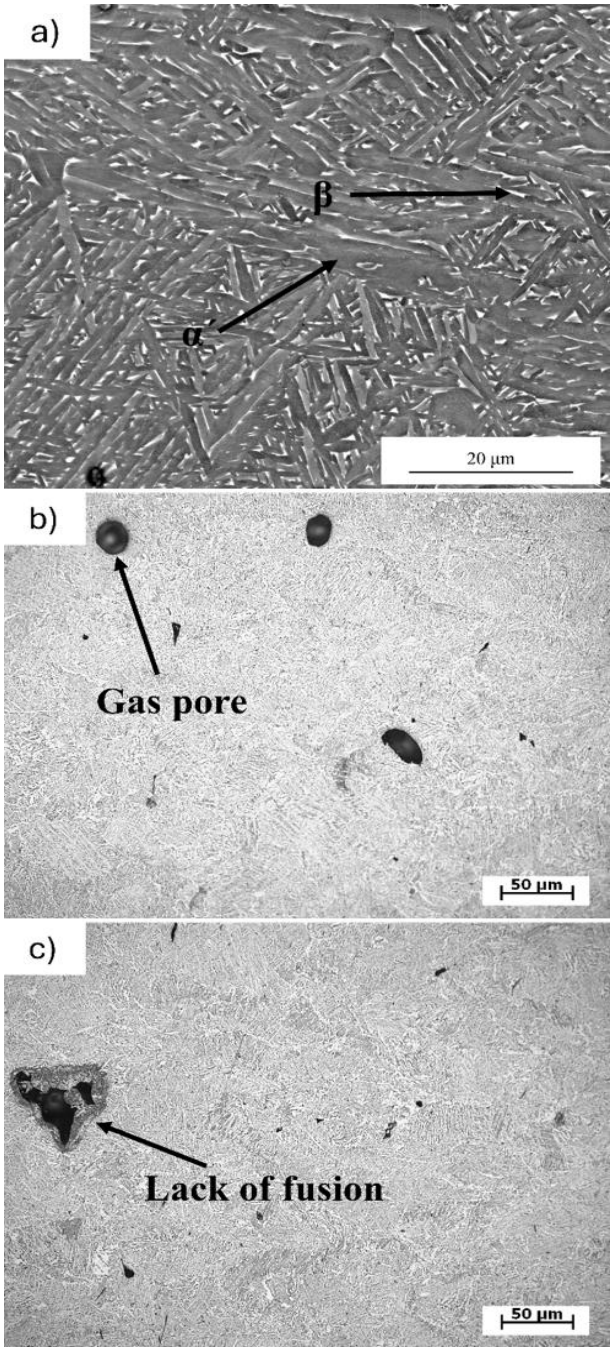

Fig. 1 *Microstructure of SLM samples a) SEM, b, c) optical*

The microstructure of the etched longitudinal sections was examined at higher magnifications using SEM in backscattered electron (BSE) mode (Fig. 1a and Fig. 2a). A uniform/homogeneous microstructure was observed across the series. The first batch was characterized by a fine acicular martensitic microstructure with varied orientation of needles (Fig. 1a). This microstructure is referred to as α´ martensite and was observed in the samples observed in [6, 16, 17]. The microstructure with varied orientation of needles is formed through a diffusionless transformation of β-phase during rapid cooling. The rapid cooling induces significant internal stresses within the martensitic needles, which hinder dislocation motion and contribute to the increased hardness and strength of the α´ martensite. It is typical for this alloy manufactured by SLM technology without subsequent heat treatment. A random distribution of martensitic needles results in enhanced strength and hardness, accompanied by reduced ductility [16], which is consistent with the measured mechanical properties (Tab. 1). The second batch exhibited a lamellar α + β microstructure (Fig. 2). This microstructure was slightly coarser compared to the first batch and is formed during heat treatment. The metastable α´ transforms into stable α + β phases at elevated temperatures. Holding at elevated temperature during HIP also leads to an in-crease in α-phase grain size, resulting in coarsening of the structure. In addition to reducing the number and size of pores, HIP also homogenizes the microstructure, which promotes a more uniform distribution of internal stresses during mechanical loading and reduces localized stress concentrations. The same transformation was observed by N. Eshawish and H. Li in [4, 18]. This microstructure is characterized by slightly lower strength but improved ductility. Due to the increased ductility while maintaining high strength that meets the standard, the HIP-treated samples are suitable for use in implantology.

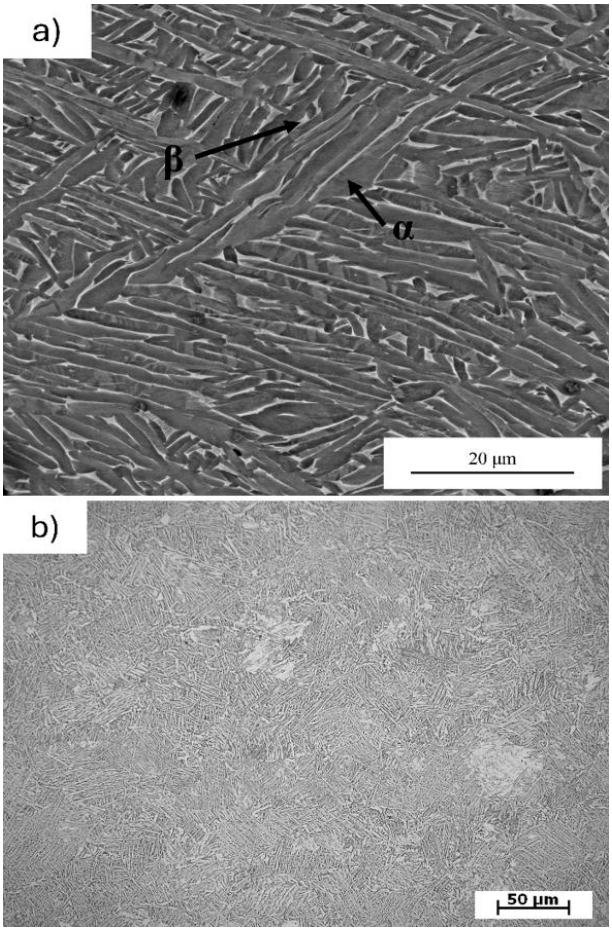

Fig. 2 *Microstructure of HIPed samples a) SEM, b) optical images*

3.3 Porosity

Surface area porosity and defect distribution were observed using optical microscopy. On the longitudinal sec-tions of the samples (Fig. 3), the polished unetched surface (bright area) is visible, with black regions correspond-ing to pores. The first batch (without heat treatment) exhibited many pores. These included gas pores, which were large and rounded, as well as smaller defects, some with a circular shape and others with irregular shapes, likely caused by lack of fusion. Cracks were also visible near the surface, most likely as a result of the uniaxial tensile test. Additionally, irregularities around the edges of the samples were observed, probably caused by surface roughness.

Samples 4 and 5 in this batch contained significantly fewer pores than the other samples. This could be due to the inhomogeneous distribution of defects within the material and the preparation of sections with fewer pores. To increase accuracy, a volumetric analysis was conducted.

The second batch (heat-treated using hot isostatic pressing) exhibited a very low amount of visible porosity. For this reason, quantification of defects using volumetric analysis was not feasible.

The porosity results, including areal porosity from metallographic examination and volumetric porosity from micro-computed tomography, are summarized in Tab. 2. The first batch exhibited significantly higher porosity and larger pore sizes compared to the second batch. Gas pores and lack of fusion defects with an average size of 11.6 ± 7.9 μm were detected. In batch No. 2, only micropores with an average size of approximately 3.5 ± 2.8 μm were observed. Which means that HIP led to a significant reduction in porosity, which may also be one of the reasons for the increased ductility after HIP. The same reduction in porosity was observed in [18].

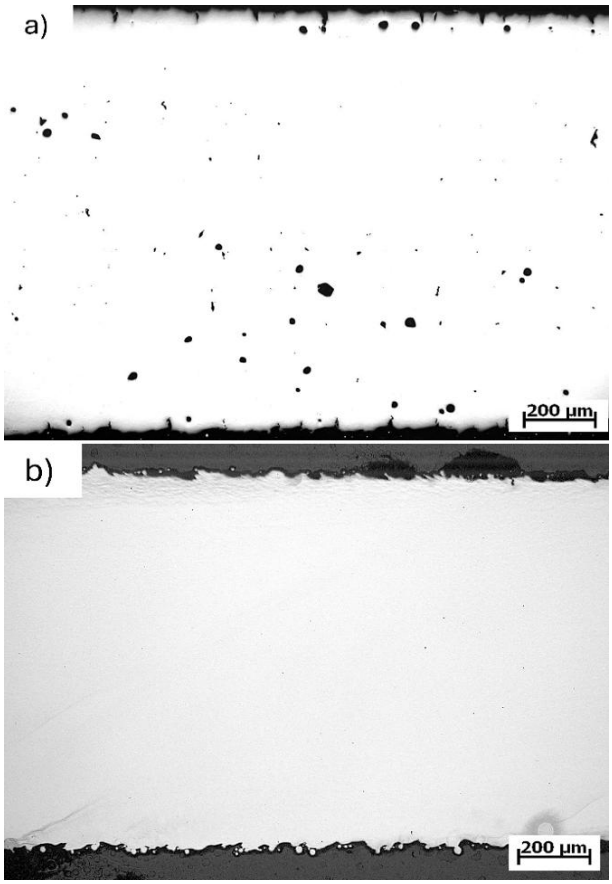

Fig. 3 *The polished unetched longitudinal sections a) SLM b) HIP*

Tab. 2 *Porosity from μCT analysis and metallographic examination*

Batch number	Sample number	Porosity [%]		Batch number	Sample number	Porosity [%]	
		μCT analysis	Metallographic examination			μCT analysis	Metallographic examination
1	1	0.37	0.27 ± 0.04	2	6	-	0.003 ± 0.003
	2	0.44	0.20 ± 0.03		7	-	0.006 ± 0.002
	3	0.37	0.29 ± 0.01		8	-	0.009 ± 0.004
	4	0.40	0.21 ± 0.02		9	-	0.014 ± 0.007
	5	0.48	0.20 ± 0.08		10	-	0.004 ± 0.003

Fig. 4 shows a 3D model of pore distribution in batch No. 1 created by μCT analysis. The observation direction is perpendicular to the build axis. The defects are concentrated in a grid-like pattern. This observed pattern can be attributed to inadequate overlap of melt pools in neighbouring scan lines, resulting from improper calibration of printing parameters [20].

Porosity was homogeneous among the samples within each series, along with the measured values of pore size and shape. In batch No. 1, the aspect ratio and Feret diameter values were determined from the measured volumetric porosity (Fig. 5). On average, the aspect ratio ranged between 0.5 and 0.6, which indicates that the defects were predominantly lack-of-fusion pores, as these have an irregular shape and therefore act as stress concentrators. The predominance of such pores is visible in Fig. 3a. Larger gas pores, unmelted surface particles and microcracks are

also present and can also act as stress concentrators. However, due to spherical shape of gas pores, they do not deteriorate the mechanical properties to the same extent [15]. A comparison of both series reveals a trend of increasing ductility as porosity decreases (Tab. 1). While the trend is evident in all samples, the ductility value is not strictly proportional to porosity, implying that additional factors contribute to the observed ductility (Fig. 6). This sample exhibited the highest porosity, but not the lowest ductility, as would be expected. The deviation from the expected correlation between porosity and ductility suggests that other microstructural factors influence mechanical behaviour [21]. Local variations in the orientation and distribution of martensitic needles, as demonstrated by the authors in [18], residual stresses introduced during SLM, was shown in [18], or small-scale microcracks may partially offset the effect of porosity [15]. In the first batch, regions with an α + β structure may appear locally due to multiple remelting events. Their non-homogeneous distribution and higher occurrence in some samples may be another reason for the increased ductility despite the high porosity [4]. Internal stresses and porosity have the greatest impact on tensile mechanical properties, whereas their influence becomes negligible under compressive loading [15]. Additionally, the shape and connectivity of pores, rather than their total volume alone, can affect the initiation and propagation of plastic deformation. These factors collectively explain why some samples with higher porosity do not exhibit the lowest ductility, highlighting the complex interplay between microstructure and defects in determining mechanical performance [4, 15, 18, 21].

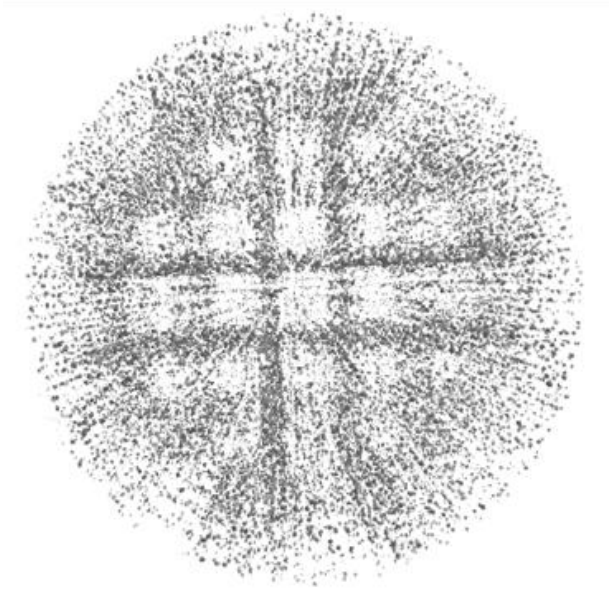

Fig. 4 *3D model of pore distribution of SLM samples from μCT*

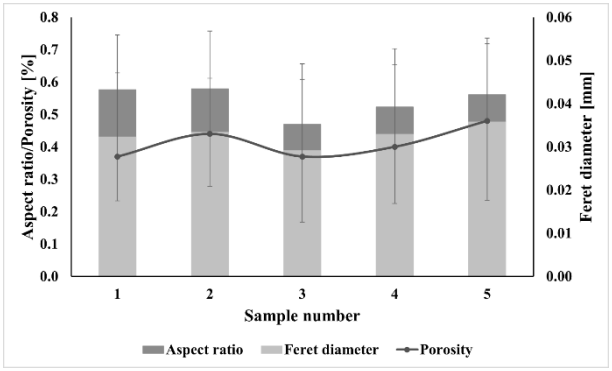

Fig. 5 *Aspect ratio, Feret diameter and porosity of SLM samples*

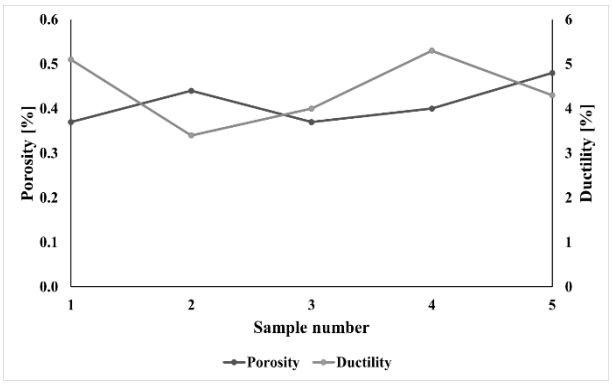

Fig. 6 *Porosity and ductility of the SLM sample*

Practically, the reduction of porosity via HIP has direct implications for biomedical applications. Lower porosity improves fatigue resistance and ensures reliability of load-bearing implants, while the maintained strength combined with increased ductility meets the requirements for orthopedic applications. This demonstrates that careful control of both SLM parameters and post-processing heat treatment is essential for producing high-quality, implant-grade components.

4 Conclusion

In this study, the porosity and microstructure of SLM and SLM+HIP samples were characterized. Three types of defects were identified. Samples after SLM contained 24 % gas pores, with the remaining pores consist-ed of sharp-edges defects such as lack of fusion defects and micropores. Samples after SLM and HIP contained only a small amount of micropores. The absence of large pores in the HIP samples resulted in lower porosity, which was one of the factors contributing to increased ductility. A relationship between Feret diameter, aspect ratio, and porosity was established through comparison. Furthermore, the expected inverse relationship between increasing ductility and decreasing porosity was observed across the series, the correlation is not strictly propor-tional, indicating that other factors also affect the measured ductility.

Additionally, the microstructure of the samples was described. The acicular martensitic α´ phase with a small amount of β phase was found in samples after SLM. The lamellar α + β phase was observed in samples after HIP.

Based on the results, it can be concluded that HIP significantly reduces porosity. Moreover, it leads to chang-es in the microstructure and, as a result, increases ductility with a slight decrease in yield strength, while maintain-ing ultimate strength and elastic modulus. For these reasons, HIP is an effective treatment of samples printed by SLM for medical applications. A remaining drawback is the unaffected elastic modulus, which remains too high for orthopaedic implant applications.

Acknowledgement

CzechNanoLab project LM2023051 funded by MEYS CR is gratefully acknowledged for the financial support of the measurements/sample fabrication at LNSM Research Infrastructure. The authors would like to thank the Ministry of Health of the Czech Republic (Project No. NW25-08-00044) and specific university research (A1_FCHT_2025_011) for financial support.

References

[1] ABD-ELAZIEM, W., et al. (2024). Titanium-Based alloys and composites for orthopedic implants Applications: A comprehensive review. *Materials & Design*, Vol. 241, pp. 112850. ISSN: [0264-1275].

[2] WAGNER, W.R., et al. (2020). *Biomaterials Science An Introduction to Materials in Medicine*, ISBN: [978-0-12-816137-1].

[3] KRIŠTOFOVÁ P, KUBÁSEK J, VOJTĚCH D, PALOUŠEK D, SUCHÝ J. (2019). Microstructure of the Mg-4Y-3RE-Zr (WE43) Magnesium Alloy Produced by 3D Printing. *Manufacturing Technology*, Vol. pp. 89-94. ISSN [1213-2489].

[4] ESHAWISH, N., MALINOV, S., SHA, W. et al (2021). Microstructure and Mechanical Properties of Ti-6Al-4V Manufactured by Selective Laser Melting after Stress Relieving, Hot Isostatic Pressing Treatment, and Post-Heat Treatment. *J. of Materi Eng and Perform*, Vol. 30, pp. 5290–5296 ISSN: [1544-1024].

[5] WEN, C. (2021). *Structural Biomaterials Properties, Characteristics, and Selection*, ISBN: [978-0-12-818831-6].

[6] MARIN, E. AND A. LANZUTTI (2023). Biomedical Applications of Titanium Alloys: A Comprehensive Review. *Materials,* Vol. 17, Basel, Switzerland. ISSN: [1996-1944].

[7] NGUYEN, H.D., et al. (2022). A critical review on additive manufacturing of Ti-6Al-4V alloy: microstructure and mechanical properties. *Journal of Materials Research and Technology*, Vol. 18, pp. 4641-4661. ISSN: [2238-7854].

[8] NGO, T.D., et al. (2018). Additive manufacturing (3D printing): A review of materials, methods, applications and challenges. *Composites Part B: Engineering*, Vol. 143, pp. 172-196. ISSN: [1359-8368].

[9] AIZA, I., et al. (2025). Effects of build orientation and inclined features on physical, microstructural and mechanical properties of powder bed fusion additively manufactured metallic parts. *Progress in Materials Science*, Vol. 147, pp. 101357. ISSN: [0079-6425].

[10] SONG, Y., et al. (2024). An overview of selective laser sintering 3D printing technology for biomedical and sports device applications: Processes, materials, and applications. *Optics & Laser Technology*, Vol. 171, pp. 110459. ISSN: [0030-3992].

[11] HORKÝ R, KUŚMIERCZAK S, NÁPRSTKOVÁ N, KAMBAROVÁ I. (2024). Effect of Heat Treatment and Corrosion Load on the Microstructure of the Ti6Al4V Alloy. *Manufacturing Technology*, Vol. 24(6) pp. 914-928. ISSN [1213-2489].

[12] YADROITSEV, I. AND I. YADROITSAVA (2021). 3 - A step-by-step guide to the L-PBF process. In: *Fundamentals of Laser Powder Bed Fusion of Metals*, pp. 39-77. Elsevier. ISBN: [978-0-12-824090-8].

[13] DU PLESSIS, A. (2121 6 - Porosity in laser powder bed fusion. In: *Fundamentals of Laser Powder Bed Fusion of Metals*, pp. 155-178. Elsevier. ISBN: [978-0-12-824090-8].

[14] SINGLA, A.K., et al. (2021). Selective laser melting of Ti6Al4V alloy: Process parameters, defects and post-treatments. *Journal of Manufacturing Processes*, Vol. 64, pp. 161-187. ISSN: [1526-6125].

[15] WANG, S., et al. (2022) Role of porosity defects in metal 3D printing: Formation mechanisms, impacts on properties and mitigation strategies. *Materials Today*, Vol. 59, pp. 133-160. ISSN: [1369-7021].

[16] BAGHERIFARD, S. AND M. GUAGLIANO (2021). 12 - Post-processing, In: *Fundamentals of Laser Powder Bed Fusion of Metals*, pp. 327-348. Elsevier. ISBN: [978-0-12-824090-8].

[17] GOSTICK, J., et al. (2016). OpenPNM: A Pore Network Modeling Package. *Computing in Science*

& Engineering, Vol. 18, pp. 1-1. ISSN: [1521-9615]

[18] LI, H., et al. (2025). Evaluation of the microstructure and mechanical properties of additive manufactured Ti-6Al-4V alloy under various heat treatment conditions: Optimization of heat treatment programme and depth of effective layer. *Journal of Alloys and Compounds*, Vol. 1026, pp. 180427. ISSN: [0925-8388].

[19] SALLICA-LEVA, E., et al. (2016). Ductility improvement due to martensite α' decomposition in porous Ti–6Al–4V parts produced by selective laser melting for orthopedic implants. *Journal of the Mechanical Behavior of Biomedical Materials*, Vol. 54, pp. 149-158. ISSN: [1751-6161].

[20] LI, J., et al. (2025). Evolution and prediction of lack of fusion pores in laser powder bed fusion process based on in-situ monitoring. *Measurement*, Vol. 245, pp. 116617. ISSN: [0263-2241].

[21] TAO, P.; ZHONG, J.; LI, H.; HU, Q.; GONG, S.; XU, Q (2019), Microstructure, Mechanical Properties, and Constitutive Models for Ti–6Al–4V Alloy Fabricated by Selective Laser Melting (SLM). *Metals*, Vol. 9, pp. 447. ISSN: [2075-4701]